ChemPubSoc Europe

DOI: 10.1002/chem.201405817

CHEMISTRY A European Journal Full Paper

Surface Chemistry

Control of the Intermolecular Coupling of Dibromotetracene on Cu(110) by the Sequential Activation of C–Br and C–H bonds

Lara Ferrighi,[a] Igor Píš,[c, d] Thanh Hai Nguyen,[b] Mattia Cattelan,[b] Silvia Nappini,[c] Andrea Basagni,[b] Matteo Parravicini,[a] Antonio Papagni,[a] Francesco Sedona,[b] Elena Magnano,[c] Federica Bondino,[c] Cristiana Di Valentin,*[a] and Stefano Agnoli*[b]

Abstract: Dibromotetracene molecules are deposited on the Cu(110) surface at room temperature. The complex evolution of this system has been monitored at different temperatures (i.e., 298, 523, 673, and 723 K) by means of a variety of complementary techniques that range from STM and temperature-programmed desorption (TPD) to high-resolution X-ray spectroscopy (XPS) and near-edge X-ray absorption fine structure spectroscopy (NEXAFS). State-of-the-art density-functional calculations were used to determine the chemical processes that take place on the surface. After deposition at room temperature, the organic molecules are transformed into organometallic monomers through debromination and carbon-radical binding to copper adatoms. Organometallic dimers, trimers, or small oligomers, which present copper-bridged molecules, are formed by increasing the temperature. Surprisingly, further heating to 673 K causes the formation of elongated chains along the Cu(110) close-packed rows as a consequence of radical-site migration to the thermodynamically more stable molecule heads. Finally, massive dehydrogenation occurs at the highest temperature followed by ring condensation to nanographenic patches. This study is a paradigmatic example of how intermolecular coupling can be modulated by the stepwise control of a simple parameter, such as temperature, through a sequence of domino reactions.

Introduction

The fundamental understanding of the organization of molecules on surfaces is the basis of the development of new devices in organic electronics and optoelectronics.[1] Organic layers made up of aromatic molecules (e.g., acenes,[2] nanographenes,[3] rylenes,[4] porphyrins,[5] etc.) exhibit quite unique properties, such as electric conduction, the ability to interact with light, and the possible mediation of energy conversion and transfer. All these functionalities, however, are strongly connected not only to the specific chemical nature of the molecular units, but also to their connectivity.[6–9]

So far, several different types of interactions have been exploited to control intermolecular architectures on surfaces, which range from Van der Waals interactions, hydrogen bonding, or even actual covalent bonds.[10–12] Also the substrate can play a relevant role either as a catalyst that can promote the reactions between molecular units[13] or by participating directly in the molecular-assembly process by providing additional coordinating centers or by controlling the aggregation because of its anisotropic properties.[14]

Strategies aimed at connecting molecules on surfaces exploit specific active sites in the pristine molecular backbones, thus creating an interconnected structure in a bottom-up fashion. Herein, we demonstrate that it is possible to circumvent this approach and to tune the connectivity of a molecular layer in a more versatile way by carefully controlling the temperature.[9,15] Furthermore, the case of dibromotetracene (DBT) molecules on a Cu(110) surface is presented as an intriguing and paradigmatic case.

Halogenated molecules are suitable for surface polymerization because they undergo the Ullmann coupling on a proper catalytic metal substrate.[11,16,17] In particular, brominated and iodinated molecules undergo C–X (X = Br, I) dissociation on copper surfaces at room temperature (RT), and an organometallic network is usually observed owing to the catalytic activity of the metal surface. Several molecules have been tested and, independent from the molecular backbone, the C–

[a] Dr. L. Ferrighi, Dr. M. Parravicini, Prof. A. Papagni, Prof. C. Di Valentin
Department of Materials Science
Università di Milano-Bicocca
Via Cozzi 55, 20125 Milano (Italy)
E-mail: cristiana.divalentin@mater.unimib.it

[b] Dr. T. H. Nguyen, M. Cattelan, A. Basagni, Dr. F. Sedona, Dr. S. Agnoli
Department of Chemical Sciences
University of Padua
Via Marzolo 1, 35131 Padova (Italy)
E-mail: stefano.agnoli@unipd.it

[c] Dr. I. Píš, S. Nappini, E. Magnano, Dr. F. Bondino
IOM CNR, Laboratorio TASC
S.S. 14 Km. 163
5 I-34149 Basovizza (TS) (Italy)

[d] Dr. I. Píš
Elettra-Sincrotrone Trieste S.C.p.A.
S.S. 14 Km 163.5
I-34149 Basovizza (TS) (Italy)

Supporting information for this article is available on the WWW under http://dx.doi.org/10.1002/chem.201405817.

C coupling starts at 550 K and the so called protopolymer is converted into a covalent structure.[18–21] Typically, the order of the network decreases during this step due to the irreversible bond-formation conditions, and it is only possible to improve the long-range order by fine-tuning the reaction parameters.[22–24] In addition, functionalization by halogen atoms and, in particular, the choice of their positions within the molecular scaffold have been used to control the growth of the polymers.[17,25–27] Herein, we will show that the position of bromine atoms within the molecular structure affects not only the connectivity of the 2D covalent network, but also the reactivity of the isolated monomeric unit. In particular, DBT is a prototypical halogenated tetracene derivative, for which the C–C coupling step is strongly affected by steric hindrance. The surface-assisted molecular-coupling chemistry is guided by the homolytic dissociation of the C–Br bonds at low temperature, whereas the intrinsic stability of the debrominated molecules changes the expected scenario on increasing the temperature above 550 K, and the connectivity between the molecules springs toward the positions at which the radical sites are more stabilized, namely, the ends of the DBT molecules (head and tail in Figure 1, top panel). This migration from the sides to the ends causes a dramatic change in the coupling pathway, that is, from a side-to-side to a head-to-tail arrangement. Consequently, long chains are formed along the Cu(110) close-packed rows. When the temperature is further increased, the dehydrogenation processes take over and nondirectional cyclodehydrogenation reactions promote the formation of defective nanographenic patches.

This study has been performed by tightly combining four complementary techniques: STM imaging, temperature-programmed desorption (TPD) experiments in ultrahigh vacuum (UHV), high-resolution (HR) X-ray spectroscopy (XPS), near-edge X-ray absorption fine structure (NEXAFS) spectroscopy, and state-of-the-art computational methods based on density-functional theory (DFT).

The exploitation of different surface reactions and the careful design of the molecular precursors can open the way to a more global approach to control the connectivity of 2D covalent networks. In particular, a detailed understanding of surface phenomena can enable dynamic control over surface nanophases by varying a simple macroscopic parameter such as temperature.

Results and Discussion

Deposition at room temperature

STM was first used to follow the growth of DBT films on a Cu(110) surface at varying temperatures. Initially, the exposure of the Cu(110) surface to a submonolayer amount of DBT was carried out at room temperature. Single molecular units were observed in terms of a distinct STM contrast with a central rod, which corresponds to the central tetracene moiety, and two bright spots on the sides, which correspond to the 5,11 positions of the carbon backbone (see top panels in Figure 1 for the DBT sketch and the experimental STM images). These

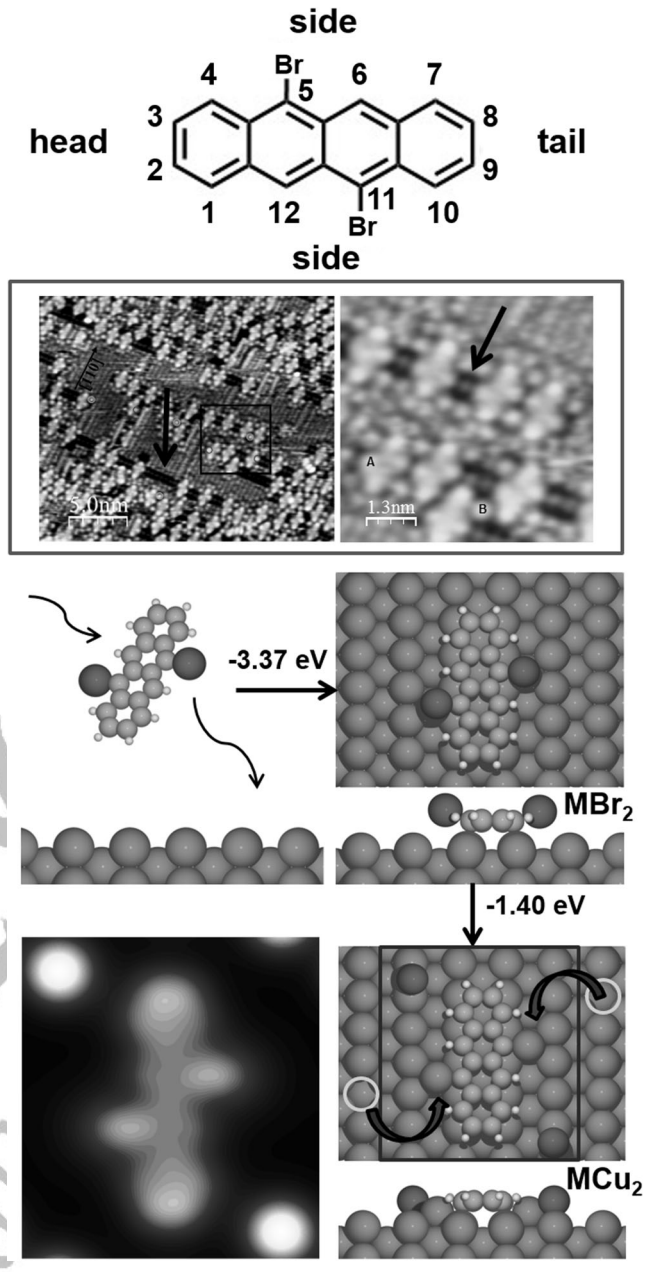

Figure 1. Deposition at room temperature. Top panels: DBT sketch and experimental STM images of 0.5 ML DBT deposited at room temperature. The circles ("A" in the inset) correspond to copper atoms bonded to the tetracene unit, whereas squares ("B" in the inset) correspond to bromine atoms and the arrow indicates copper vacancies ($V_{bias} = -0.7$ V, $I = 46.5$ nA 25×21.2 nm^2). Lower panels: DFT models of the reaction path and simulated STM image. The DBT molecule is first deposited on the Cu(110) surface (MBr_2) and immediately undergoes debromination, thus leaving radical carbon atoms that are saturated by copper adatoms (MCu_2). The gray circles indicate the copper vacancies. The simulated STM image, at a bias of −0.7 V, is reported for the MCu_2 structure on the bottom left panel.

molecular species are randomly scattered on the surface and do not decorate the step edges or other morphological features. Moreover, it is possible to observe the presence of bright spots on the surface that are either isolated or form linear chains in amounts that are about twice the number of the molecular units. The tetracene units lie flat on the surface

and are perfectly aligned with the [$\bar{1}$10] direction of the substrate, in agreement with previous reports on the growth of pure tetracene on Cu(110) surfaces.[28,29]

Furthermore, the substrate morphology is strongly affected by the deposition of DBT molecules, as evidenced by the formation of vacancy islands and small pits that were not noticeable prior to the deposition (see the black arrows in Figure 1).

Most of the above observations can be interpreted on the basis of DFT calculations. The reaction pathway and the energy variations associated with the corresponding processes are represented in Figure 1. The binding energy of the as-deposited molecule to the copper surface amounts to about −3.4 eV (MBr_2 in Figure 1; see the Experimental Section for the nomenclature), which is a value very close to the values reported previously.[30]

The DBT deposition on the surface is followed by prompt debromination (because of which no as-deposited DBT was experimentally observed with STM) and replacement by copper atoms extracted from the substrate (i.e., MCu_2 in Figure 1), thus forming a surface organometallic compound and leaving copper vacancies on the top layer (light-gray circles in Figure 1). This process is accompanied by a further energy gain of −1.4 eV and can be decomposed in few consecutive steps: first and second debromination (−1.02 eV), copper-adatom formation (+1.49 eV), and carbon-radical saturation by copper adatoms (−1.88 eV; see Figure S1a in the Supporting Information). The simulated STM image of the final species present on the surface (i.e., the organometallic complex and adsorbed bromine atoms) is reported in the left bottom panel of Figure 1. The agreement of this image with the experiments is excellent: the monomers present bright spots at the sides (i.e., Cu adatoms) and at the ends of the molecule, this latter effect is due to an upward lateral bending of the tetracene molecular plane[31] (see Figure S1b in the Supporting Information). The surface bromine atoms are very bright, thus confirming the experimental assignment.

Interestingly, the experimental STM topographies indicate that the copper bright spots on the tetracene units are in the 5,11 position in most cases (i.e., where the Br atoms were originally bonded), but a few 5,12 and 5,10 geometries (about 30%) are present and in greater quantities than in the starting material (10%). This finding suggests that the carbon- radical sites, which are formed after the debromination reaction, must be rather stable due to the interaction with the copper surface, although a few of these sites might move to■■OK?■■ the adjacent carbon atom of the tetracene unit.

The vision outlined above is in agreement with previous reports in which similar halogenated molecules were dosed on metal surfaces[32] and is also supported by photoemission data (Figure 2).

The C 1s spectrum measured at room temperature (Figure 2a, bottom spectrum) can be divided into four components (see the Materials and Methods for details about the multipeak analysis). The main components B and C, centered at a binding energy (BE) of 284.0 and 284.4 eV, are typical spectral features for submonolayer amounts of polyacenes on copper surfaces.[33,34] The origin of the energy separation of these two components can be deduced from the distances between the carbon atoms and their nearest copper-atom neighbors in the substrate. Different adsorption sites of the single carbon atoms influence the extent of molecule–metal hybridization, thus resulting in site-dependent contribution to the C 1s core-level shift. Thus, the C 1s component B at a BE of 284.0 eV was assigned to carbon atoms only bonded to other carbon atoms (average C–Cu distance: ca. 2.21 Å) and component C at a BE of 284.4 eV was assigned to carbon atoms bearing hydrogen atoms (C–Cu distance: ca. 2.35 Å from DFT calculations). In addition to these two main C 1s components, typical for nonfunctionalized polyacenes, the extra component A was observed at 283.3 eV after the DBT deposition, which is indicative of C–Cu bonds (typically between 283 and 284 eV)[21,35–37] and confirms that the biradical species that result from the debromination bind to copper adatoms, thus forming surface organometallic complexes. We also observed a small C 1s component at a BE of 285.5 eV (component D). This feature can possibly be attributed to a residual interaction between the leaving bromine atoms and the tetracene C–H groups, which could persist at low temperature. The absence of the high energy C 1s component at a BE of 286.6 eV, typical of C–Br bonds (see Figure S2 in the Supporting Information), confirms the full debromination of the DBT at room temperature. The same evidence is given by the line for the Br 3d photoemission (Figure 2b). Two components with a Br $3d_{5/2}$ peak maximum centered at a BE of 68.4 and 69.0 eV (components 1 and 2, respectively) are indicative of bromine atoms detached from the organic molecules on copper substrates.[21,35]

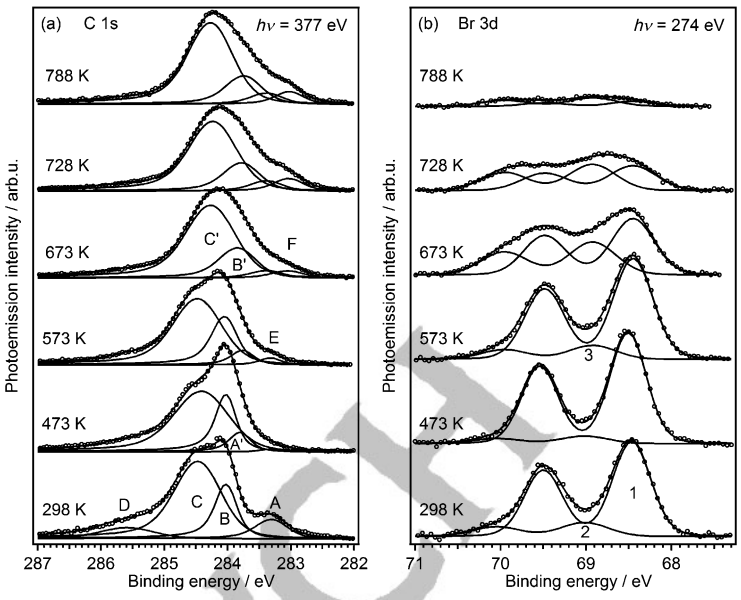

Figure 2. a) C 1s (left) and b) Br 3d (right) core-level photoemission spectra recorded after the deposition of DBT on the Cu(110) surface at room temperature and after the subsequent stepwise heating to 788 K (from bottom to top). See the main text for the peak assignments.

After annealing above 473 K, we observed a third component (component 3) with a maximum at 68.9 eV. This component becomes the dominant feature of the Br 3d spectrum after annealing at high temperatures, thus corresponding to the formation of linear chains along the [$\bar{1}$10] direction, as observed in STM images. Thus, we tentatively assign this third component to the bromine adatoms grouped in linear chains. The chains can be composed solely of bromine atoms, similar to 2D Br islands formed on a Cu(111) surface at similar temperatures[25,38] or they can consist of alternate -Br-Cu- 1D chains similar to those observed on a Pt(110) surface.[39] The corresponding BrCu compound[40] is expected to have the Br $3d_{5/2}$ peak maximum centered at 69.2 eV,[41] which is close to the value of component 3. Further investigation will be required to definitely answer the true composition of the 1D chains.

Heating to 523 K

When the DBT deposited surface is heated up to 523 K, dimers, trimers, and longer organometallic oligomers can be formed by cross-linking tetracene units with copper atoms along the [001] direction (see the top panels in Figure 3). These processes are estimated to be thermodynamically favorable because the aggregation of monomers releases copper adatoms that may go back and fill the surface vacancies on the substrate. In these oligomeric structures, the molecules maintain their main axis parallel to the [$\bar{1}$10] direction and are spaced by 0.7 nm in the perpendicular direction. This arrangement indicates that the molecules are adsorbed on every alternate row of the substrate, with single bridging copper atoms in between. The oligomer subunits in general share the same registry along the [$\bar{1}$10] direction (black rectangle in Figure 3), or they are shifted along this same direction to form staggered structures in some cases (white rectangle in Figure 3). Different from other similar systems (e.g., terphalic acid on Cu(110))[42] the type of cross-linking does not depend on the coverage; that is, there is always a single copper atom that connects two dehalogenated molecules. On the contrary, the coverage significantly affects the growth morphology; consequently, the surface crowdedness that results from a coverage close to sat-

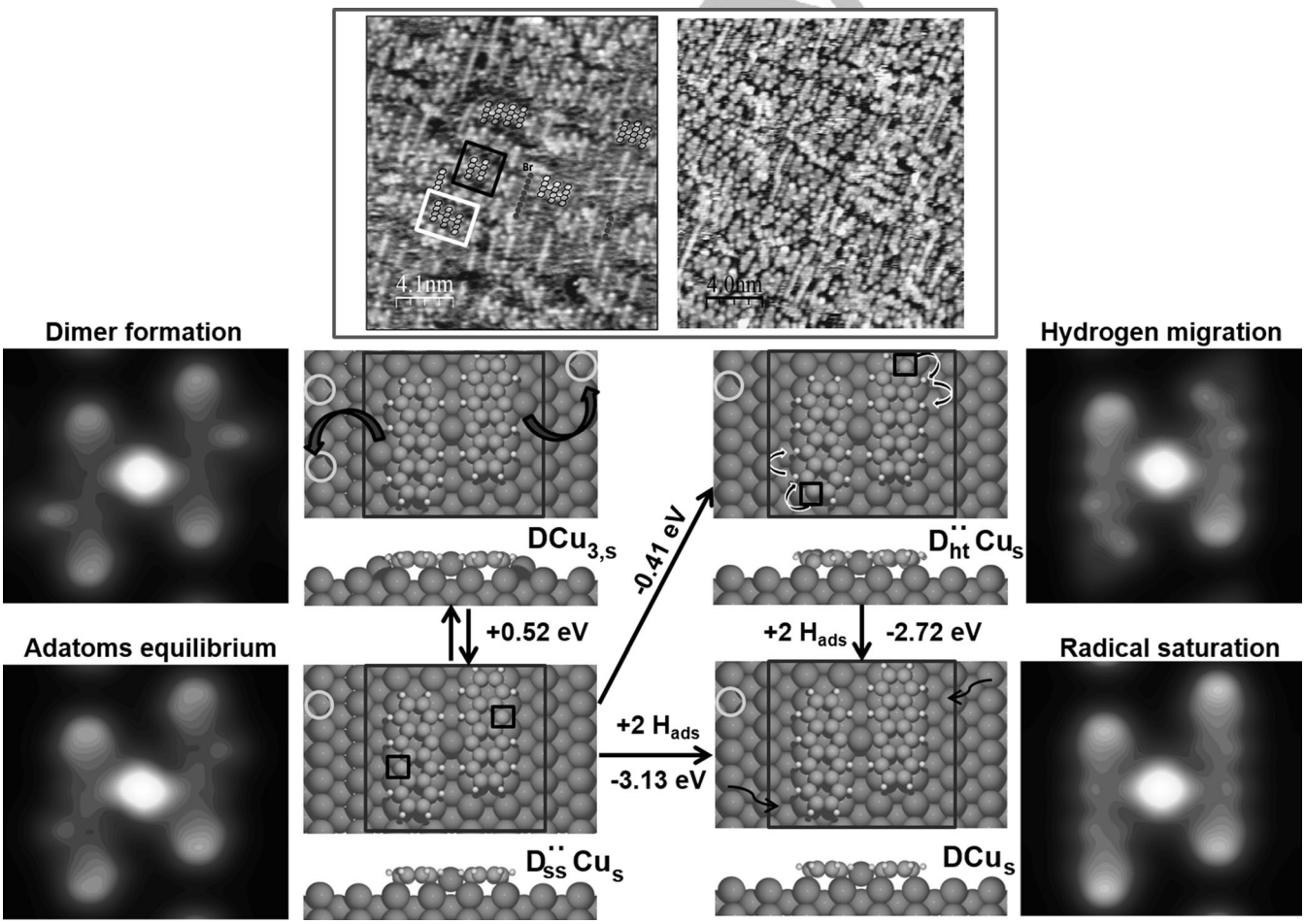

Figure 3. Heating to 523 K. Top panels: experimental STM images. Left: 0.5 ML DBT on the Cu(110) surface. The different types of oligomer are shown and the adsorbed bromine atoms are represented by dark spheres ($I = 11.49$ nA, $V_{bias} = -0.80$ V, 20×20 nm^2). Right: 1 ML DBT deposited at room temperature and annealed at 523 K ($I = 42.27$ nA, $V_{bias} = -1.54$ V, 20×20 nm^2). Central and lower panels: DFT models of the reaction processes and simulated STM images. Dimers are formed on the surface that involve three copper adatoms ($DCu_{3,s}$). The external copper adatoms could fall back into the copper vacancies (light-gray circles) present on the surface, thus leaving two carbon-radical sites (black squares) on the dimer $D^{\bullet\bullet}_{ss}C_s$. The hydrogen atoms on the molecules could rearrange, thus moving the radical sites to the heads of the molecules ($D^{\bullet\bullet}_{ht}C_s$). Atomic hydrogen adsorbed on the surface could also saturate the radical species in $D^{\bullet\bullet}_{ss}C_s$ and $D^{\bullet\bullet}_{ht}C_s$, thus producing DCu_s. The simulated STM images, at a bias of -0.7 V, are reported for each structure.

uration prevents the formation of extended oligomers because of the lack of space for an efficient mutual rearrangement of the polymer units. It is well known that the presence of adsorbed bromine atoms hinders the diffusion of molecules.[36] Therefore, a large fraction of single monomers can still be observed for coverage of around 1 ML, even at 523 K (Figure 3). In addition, most of the oligomers observed after annealing do not present the bright spots on the outer sides of the terminal molecules, whereas almost every monomer exhibited two copper bright spots after the low-temperature preparation. This result seems to indicate that the copper atoms are removed from the sides of terminal molecules and are maintained just when they bridge two tetracene moieties.

If we assume that the C–Cu bonds are labile, especially with temperature, with the copper adatoms migrating back and forth into and from a vacancy left on the surface (equilibrium between configurations $DCu_{3,s}$ and $D^{\bullet\bullet}_{ss}C_s$ in Figure 3), we can put forward two hypotheses that lead to two types of organometallic dimer: 1) one dimer with radical sites at the head and tail or 2) one dimer with hydrogen-saturated radical states ($D^{\bullet\bullet}_{ht}C_s$ and DCu_s, respectively, in Figure 3). Configuration $D^{\bullet\bullet}_{ht}C_s$ is due to the atomic-hydrogen migration from the molecular ends to the sides, whereas DCu_s results from saturation with the unavoidable H_2 molecules present in the experimental chamber.

Configuration $D^{\bullet\bullet}_{ht}C_s$ is computed to be about −0.4 eV more stable than configuration $D^{\bullet\bullet}_{ss}C_s$, whereas configuration $DCu_{3,s}$ benefits from the C–H-bond formation by about −3.1 eV. The simulated STM images of both these situations are compatible with the experimental images because no outer-side bright spots are present. It is relevant to stress that once the radical sites have migrated to the heads of the molecules, as in $D^{\bullet\bullet}_{ht}C_s$, the C–C ■■OK?■■ dangling bond does not point in the direction of an ideal adsorption site for copper adatoms, which preferentially sit between two metal rows.

The morphological changes observed by STM have also got a direct counterpart in the photoemission data (Figure 2). In fact, a decrease in the intensity of the C 1s component A is observed after the annealing between 473 and 573 K and a new C 1s component A′ at a BE of 283.8 eV appears at the same time. On the basis of the STM observations, we assigned the intensity shift from the A to A′ component to the formation of the organometallic dimers and longer oligomers. Components A and A′ correspond to the same carbon atoms within the DBT molecule, but the copper atoms that link the DBT molecules in the chains mixed with two A′ carbon atoms instead of one A atom on the sides of the organometallic complexes. The shift toward higher BE values indicates that less charge is donated to the two carbon atoms bonded to the central copper atom. This shift in the spectral intensity from A to A′ correlates very well with the STM images, thus indicating that most of the oligomers do not present copper atoms bonded to terminal tetracene units. Finally, the new C 1s component E appears at a BE of 283.4 eV in the spectra taken at 573 K. Because the intensity of these states further increases at higher temperatures, at which the level of surface disorder is higher, we can relate this feature to atomic defects in the carbon nanostructures, such as single and double vacancies and the Stone–Thrower–Wales defect.[43,44]

Heating to 673 K

Upon further annealing at 673 K, the experimental STM topographies evidence the formation of wavy oligomeric chains (see left panel in Figure 4), whereas the organometallic monomers and oligomers disappear. These chains run predominantly along the [$\bar{1}$10] direction and are one molecule wide; however, regions constituted by more compact structures can be observed as well. On the bare copper terraces, some bright spots can be observed, thus indicating the residual presence of bromine atoms, but in a smaller amount than in the films prepared at room temperature, thereby confirming the photoemission results and the TPD data (see Figure S3 in the Supporting Information) that place the desorption onset of bromine atoms as HBr just below 700 K for a submonolayer coverage. The STM images point to a dramatic change in the connectivity between the molecules, which now involves the carbon atoms in the head and the tail (3,2 and 8,9 positions). On a closer look, some of the polymeric chains, especially those running along the [$\bar{1}$10] direction, present broad evenly spaced bright spots, in which the single tetracene units are joined (Figure 4). In other cases, the polymeric chains are not confined to the same [$\bar{1}$10] row of the substrate, but make a turn and shift to an adjacent row. The combination of these two polymerization schemes is responsible for the overall new morphology that can be observed from large-scale STM topographies.

TPD spectra (Figure 5) prove that at these temperature-dehydrogenation reactions are possible, but still limited, and therefore the steric hindrance between the hydrogen atoms on the sides of the tetracene molecules prevents a potential cyclodehydrogenation reaction between two molecules on adjacent rows, such as in the geometry typical of oligomers. On the contrary, the change of the C–C coupling site from side carbon atoms, such as in the organometallic oligomers, to head/tail positions should be traced back to the aforementioned migration of radical sites or to quick hydrogenation/dehydrogenation processes at carbon atoms in different molecular positions.

Actually, the detachment of copper or hydrogen atoms can produce new radical species that can move, by virtue of the relatively high temperature, toward the thermodynamically more stable terminal rings (3,2 and 8,9 carbon atoms; see Figure 6). This migration is not unexpected considering that 2-substituted naphthalene derivatives are more stable than 1-substituted derivatives.

By starting from configurations $D^{\bullet\bullet}_{ss}C_s$ and DCu_s (Figure 3), some copper adatoms that bridge two molecules are expected to move back and forth into and from a surface copper vacancy at this temperature (in equilibrium with monomeric biradicals $2M^{\bullet\bullet}_{ss}$ and radicals $2M^{\bullet}_{s}$; Figure 6). The thermodynamically favorable hydrogen migration leads to the configuration $2M^{\bullet\bullet}_{hh}$ or $2M^{\bullet\bullet}_{th}$ from $2M^{\bullet\bullet}_{ss}$ and to $2M^{\bullet}_{h}$ from $2M^{\bullet}_{s}$. It is evident from the energy variations that the path on the right, outlined by bold

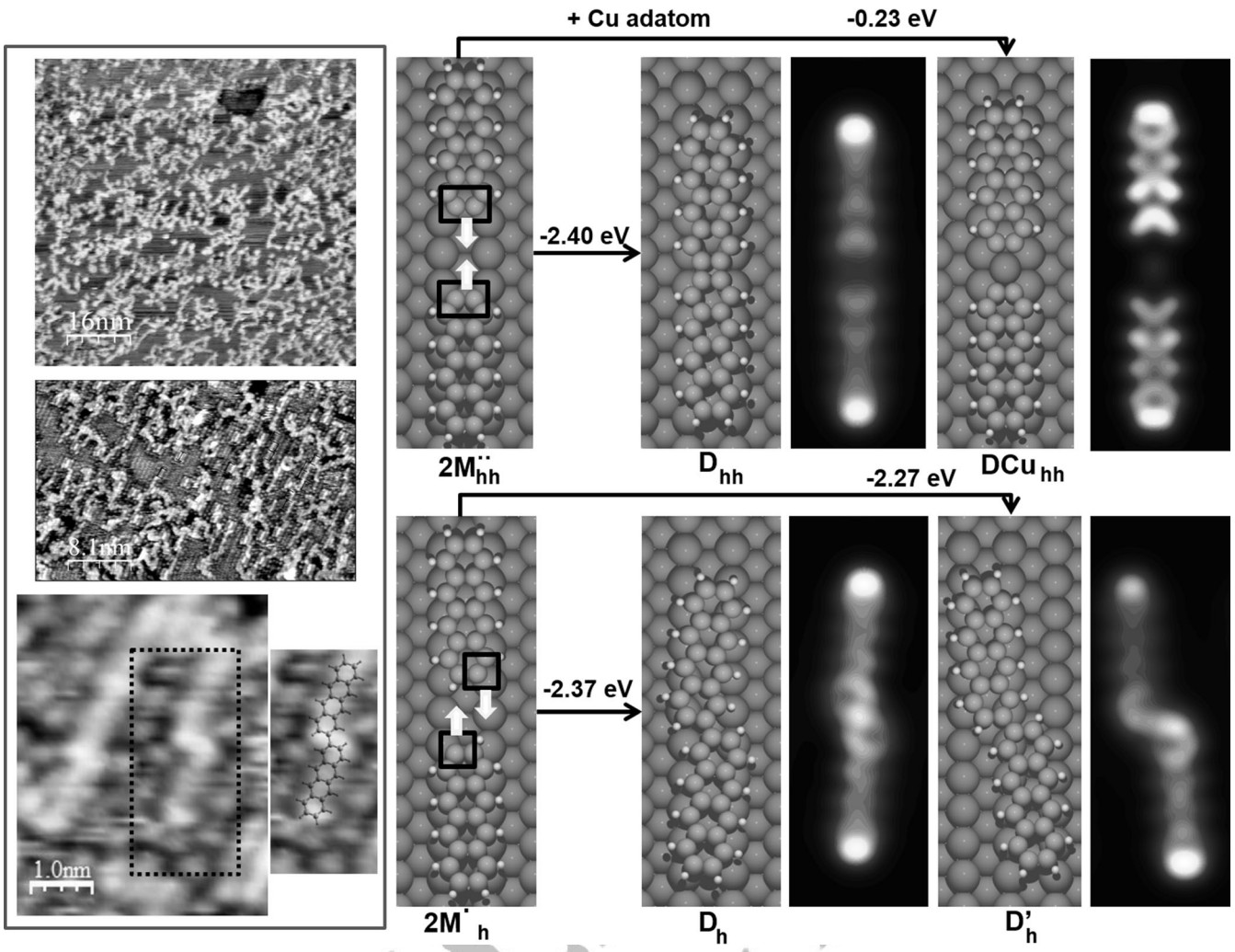

Figure 4. Heating to 673 K. Left panels: experimental STM images. Top: $I = 20.35$ nA, $V_{bias} = -1.31$ V, 20×20 nm^2; middle: $I = 11.49$ nA, $V_{bias} = -0.94$ V, 25×40 nm^2; bottom: $I = 11.49$ nA, $V_{bias} = -0.94$ V. Right panels: DFT models and the corresponding simulated STM images (bias $= -0.7$ V). Species $2M^{\bullet\bullet}_{hh}$ can clip along the same row in the [$\bar{1}$10] direction, thus forming two C–C bonds or through a copper adatom (D_{hh} or DCu_{hh}). The more-stable species ($2M^{\bullet}_{h}$) can clip either along the same row or bridge two adjacent rows in the [$\bar{1}$10] direction (D_h or D'_h).

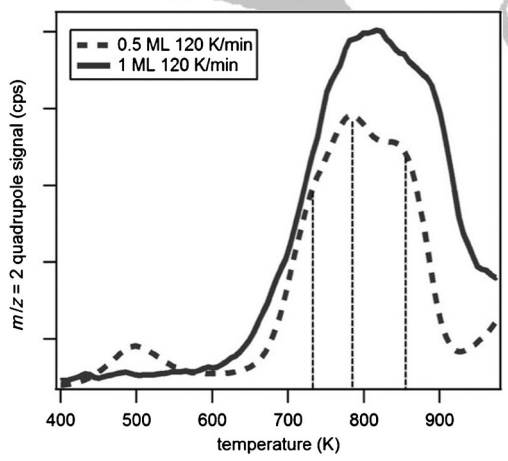

Figure 5. Desorption spectrum of hydrogen obtained by annealing at 2 K s^{-1} that shows a partial layer (0.5 ML, dotted line) and a fully covering layer (1 ML, continuous line) of DBT on the Cu(110) surface.

arrows is more advantageous, thus making monomer radicals with radical sites at the heads ($2M^{\bullet}_{h}$) the most common species on the surface at 673 K. The diffusion of these species along the [$\bar{1}$10] rows is expected to be quite fast at such temperatures, so the probability that two of these species will meet on the surface is high. What happens then is represented on the right side of Figure 4. When two tetracene biradicals $2M^{\bullet\bullet}_{hh}$ meet, dimers with or without an atomic-copper linker could be formed. Most probably, two single-radical tetracene species are present on the surface $2M^{\bullet}_{h}$, which may form dimers, thus bridging two adjacent [$\bar{1}$10] rows (models D'_h and D_h). Both simulated STM features of bridging dimers are clearly visible in the zoomed area of the experimental STM topography at the bottom of the left panel in Figure 4. Finally, we exclude the possible presence of a copper adatom because of the much worse agreement of the simulated STM contrast with the experiment and on the basis of photoemission results (see below).

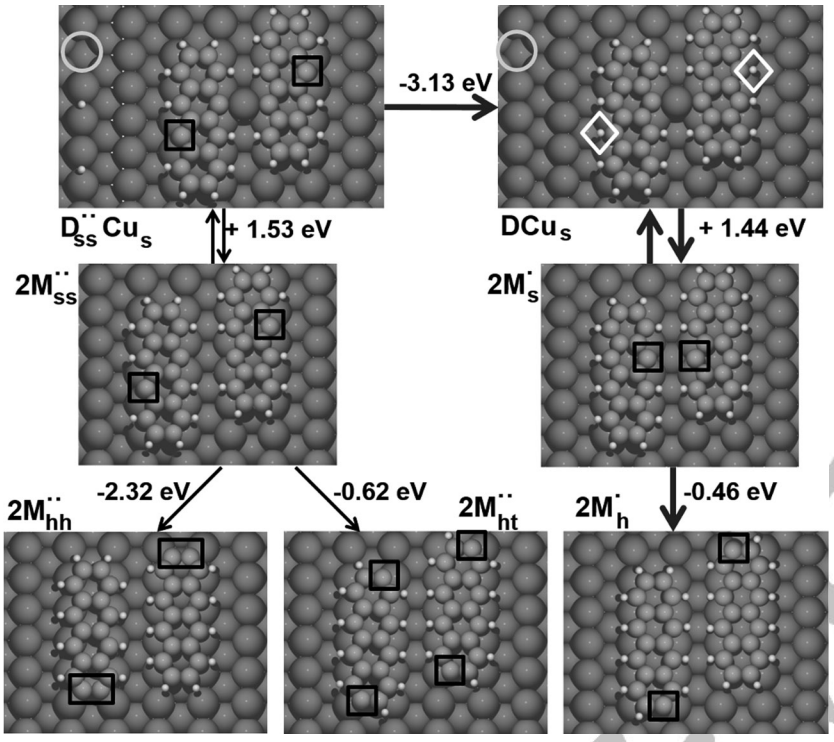

Figure 6. Schematic representation of the species present on the surface at 673 K. At this high temperature, some copper adatoms in the organometallic dimers $D_{ss}^{\bullet\bullet}C_s$ or DCu_s could fall back into the surface vacancies (light-gray circles) and leave two additional radical carbon atoms (black squares in $2M_{ss}^{\bullet\bullet}$ or $2M_s^{\bullet}$, respectively). The radical site in $2M_{ss}^{\bullet\bullet}$ could migrate either to the same heads ($2M_{hh}^{\bullet\bullet}$) or to the opposite sides of the molecule ($2M_{ht}^{\bullet\bullet}$).The atomic-hydrogen ■■OK?■■migration in $2M_s^{\bullet}$ leads to the formation of the most stable structure $2M_h^{\bullet}$ at this temperature. The hydrogenation of the radical sites in $D_{ss}^{\bullet\bullet}C_s$ leads to the saturated DCu_s species (white diamonds).

This reaction scenario is confirmed by the photoemission measurements. As evident in Figure 2, the C 1s spectrum changes considerably upon annealing to 673 K. In particular, both the main components are shifted about 0.2 eV toward lower BE values and the intensity ratio between the main components B′ and C′ is significantly enhanced in favor of the high BE component C′. The energy shift is due to a change in the adsorption site of the carbon atoms of the newly formed molecular species with respect to the organometallic complexes, in agreement with the models depicted in Figures 4 and 5.

We ascribe the increase in the intensity of the C versus B component to the change in nonequivalent positions of the carbon atoms or to an emerging C 1s component associated with C–C coupling between the monomers, the binding energy of which is expected between 284.4 and 285 eV.[21,45,46]

Polymeric structures, similar to those observed in the present study after annealing at 673 K, have also been recently observed in the case of submonolayer amounts of quaterphenyl molecules deposited on a Cu(110) surface and annealed at a temperature of 500 K.[47] In that case, it was demonstrated that the substrate can activate the C–H bond and induce selective dehydrogenation at the heads and tails of the quaterphenyl molecules, which is followed by intermolecular aryl–aryl coupling. The resulting film morphology is characterized by wavy polymeric chains aligned with the [$\bar{1}$10] direction, similar to the results observed in this study.

Heating up to 723 K

After annealing at 723 K, the morphological changes of the surface are even more dramatic, that is, very compact shapeless islands are formed (Figure 7). The thickness of the new features still corresponds to a single molecular layer; however, it is not possible to recognize the resemblance of the single tetracene unit anymore. The resulting film can be considered to be made up of highly defective nanographene patches formed by different polycyclic aromatic hydrocarbon molecules stitched together without any long-range order.[48] Proof of massive dehydrogenation reactions comes from the H_2 desorption spectra, which show the presence of three distinct features at 745, 780, and 830 K, better resolved in the low-coverage preparation. The simultaneous loss of multiple hydrogen atoms from the tetracene molecules, especially on the sides, opens a low-energy path toward C–C coupling reactions, which was prohibited at lower temperature because of repulsive interaction between hydrogen atoms. We show one possible model of two condensed molecules and its simulated STM image in Figure S4 (see the Supporting Information). Analogous small seedlike bright features, as in the experimental topographies, are present, which can be tentatively assigned to C–C fragments. At this temperature, the bromine atoms disappear from the surface, as do the copper atoms that were embedded in the organometallic polymers. This behavior is confirmed both by XPS data, which show a massive suppression of the signal of the Br 3d core levels, and by TPD data that clearly show the presence

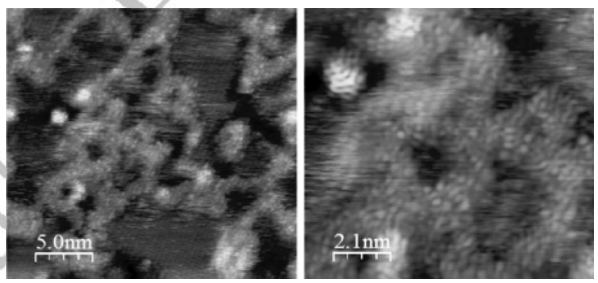

Figure 7. Heating to 723 K. Top panels: experimental STM images. Left: $I = 20.35$ nA, $V_{bias} = +0.21$ V, 25×25 nm^2; right: $I = 20.35$ nA, $V_{bias} = +0.21$ V, 10.4×20.4 nm^2.

of a strong desorption peak connected to HBr data at 750 K (see Figure S3 in the Supporting Information). Photoemission spectroscopic analysis fully corroborates the formation of a very disordered nanographene layer: the C 1s components due to defects E and F become more intense and the intensity ratio between the C and B components also slightly increases. Moreover, NEXAFS spectroscopy confirms the flat-lying geometry of the molecules that constitute the film (see Figure S5 in the Supporting Information).

Conclusion

By using a combination of experimental and theoretical methods, we characterized the structural and chemical evolution of ultrathin organic layers of DBT molecules on a Cu(110) substrate as a function of the temperature. The DBT molecules undergo an easy debromination at room temperature that leads to the creation of organometallic species along the [001] direction, in a similar way to other halogenated precursors deposited on different metal surfaces.[7,10,21] STM images and DFT calculations demonstrate that when the temperature is substantially increased, the radical species formed in the previous step can move along the molecular backbone and reach a new more stable position. Interestingly, this very unusual behavior can be observed over a significantly wide temperature range (i.e., above 673 K), in which surface-promoted dehydrogenation reactions also start to be activated.

The combination of these two factors (i.e., radical-site migration and surface-catalyzed dehydrogenation) has the overall effect of changing the connectivity within the organic layer and leads to the formation of intermolecular C–C bonds along the [$\bar{1}$10] direction. The dehydrogenation reactions are so quick and massive at higher temperature (723 K) that the radical molecules react without following a specific pathway and eventually form a patchy graphene layer. These results show how, under proper conditions, even a simple design of the molecular precursor, such as with one type of functional group, can lead to multiple coupling schemes by exploiting the intrinsic molecular stability as an additional parameter.

In conclusion, we wish to stress that two different approaches for the realization of 2D covalent networks have been combined in the present study: a well-established method based on halogen-functionalized molecules[7,8,21,27] and the emerging pathway based on specific activation of the C–H bond.[47]

Experimental Section

Synthesis of DBT

The synthesis of 5,11-dibromotetracene was carried out by electrophilic bromination with *N*-bromosuccinimide (NBS) in $CHCl_3$/DMF, as described by Müllen and co-workers.[49] The 5,12-dibromotetracene regioisomer was formed in less than 10% yield. Pure 5,11-dibromotetracene can be obtained by crystallization from toluene, and the oxidation byproducts (tetracenequinone) were easily removed by filtration of the crude mixture from the bromination reaction over a bed of SiO_2.

Preparation of DBT thin films on Cu(110)

The Cu(110) single-crystal was cleaned by repeated cycles of 0.75 keV Ar^+-ion sputtering and annealing in vacuum at 800 K until the sharp Cu(110)–(1×1) low-energy electron-diffraction (LEED) pattern was visible, and no presence of atomic carbon nor oxygen were observed in the photoemission spectra.

DBT molecules were deposited on the Cu(110) surface by using thermal sublimation from a resistively heated crucible (363 K). The base pressure during the deposition was 1.5×10^{-9} mbar. After the exposure at RT to DBT, the surface was annealed for 5 min at the targeted temperature and allowed to cool.

UHV characterization

STM: The constant-current topographic images were recorded on a VT Omicron STM in a UHV chamber that operated at the base pressure of 10^{-10} mbar. All the images were taken at RT by using chemically etched Pt–Ir tips. Typical tunneling parameters: bias = −0.7÷−1.3 V and current = 11÷42 nA.

TPD: The TPD spectra were acquired in a custom-built UHV system that operated at the base pressure of 1×10^{-10} mbar and was equipped with a mass quadrupole (HIDEN), electron analyzer, LEED, and facilities for sample cleaning and gas dosing. Heating was achieved by flowing a current through two tantalum wires and clamping the sample edges. A linear heating ramp was provided by a Eurotherm PID. The TPD spectra were collected by bringing the sampling aperture of the mass-spectrometer (diameter = 2 mm) to a few millimeters from the sample.

XPS and NEXAFS: High-resolution soft XPS and NEXAFS spectroscopy were carried out with the BACH beamline at the Elettra synchrotron (Trieste, Italy) in an UHV system that consists of a preparation chamber (1×10^{-9} mbar) and an analysis chamber (5×10^{-10} mbar) equipped with a Scienta R3000 (VG Scienta) hemispherical electron-energy analyzer.

The sample normal, the synchrotron-radiation beam, and the analyzer axis were all in the same horizontal plane. During the photoemission measurements, the crystal orientation was at a normal-incidence geometry with the photoemission angle at 60°. A photon energy of 274 eV was employed to excite the Cu 3p and Br 3d core levels, whereas a photon energy of 377 eV was used for the C 1s photoemission. A total energy resolution of 0.15 eV for both photon energies was calculated from the width of the Fermi edge. All the BE are referenced to the Fermi level, as measured at each photon energy. The Br 3d spectra were decomposed into Voigt doublet lineshapes, and the C 1s spectra were fitted with Doniach-Šunjić line shapes convoluted with a Gaussian profile.

The NEXAFS C K-edge spectra were measured in the partial-electron-yield mode that recorded the C KVV Auger yield by using the electron-energy analyzer fixed at a kinetic energy of 260 eV and with a pass-energy set to 100 eV. The raw NEXAFS spectra were normalized to the intensity of the photon beam, measured by the drain current on a reference grid located between the sample and the last focusing mirror of the beamline. The corresponding background spectra of the clean Cu(110) sample recorded under identical conditions were subtracted. Polarization-dependent measurements were performed by rotating the sample between normal-incidence geometry (angle between the sample surface plane and X-ray polarization vector: $\theta = 0°$, s-polarization) and grazing-incidence geometry ($\theta = 60°$, *p*-like polarization).

DFT calculations

The adsorption of DBT molecules on a Cu(110) surface was modelled by using the recent Van der Waals density functional vdW-DF2^{C09x},[50] which has been proven to give the best performance for the adsorption distances of graphene on metal surfaces. The nomenclature used in the text and Figures 3, 4, and 6■■OK?■■ for the species adsorbed on the Cu surface is the following: M = monomer, D = dimer, Br = bound Br atom, Cu = bound Cu atom, = C = dangling bond, s = side, h = head, t = tail (for example, a DBT molecule on the surface is MBr_2).

Supercells of 4×6, 5×6, and 3×12 were used, with a vacuum of about 20 Å perpendicular to the surface to avoid interaction between the images. The Cu surface was modeled by five-layer slabs with 48, 60, or 72 atoms per metal layer, in which the top three layers and the adsorbate were allowed to fully relax, and the bottom two layers were kept fixed at the optimized lattice for vdW-DF2^{C09x} (2.52 Å). The Perdew-Burke-Ernzerhof (PBE) standard ultrasoft pseudopotentials, as implemented in the plane-wave based Quantum Espresso package[51], are used with energy cutoff points of 30 and 240 Ryd (for kinetic-energy and charge-density grids, respectively). The calculation was only performed with a Gamma-point sampling of the Brillouin zone, but a few check tests with a 2×2×1 grid were carried out, thus showing a negligible influence on the energy differences. The adsorption energy [eV] for the first step in Figure 1 is calculated as $E = E_{MBr_2} - (E_{Cu(110)} + E_{DBT})$, where E_{MBr_2} is the energy of the structure MBr_2 when a DBT molecule is adsorbed on Cu(110), $E_{Cu(110)}$ is the energy of the clean slab, and E_{DBT} is the energy of an isolated DBT molecule. All the other energies in Figure 1 are calculated as energy differences between two structures.

The STM image simulations were obtained within the Tersoff–Hamann approximation, in which the tunneling current is considered to be proportional to the integrated local density of the states in a given energy window, determined by the applied bias fixed at negative value of −0.7 V to image the full state, as carried out in the corresponding experiments. The STM images were plotted at a height above the surface of about 3 Å.

Acknowledgements

This work was supported by the Italian MIUR through the national grant Futuro in Ricerca 2012 RBFR128BEC "Beyond graphene: tailored C-layers for novel catalytic materials and green chemistry", the program "Progetto Premiale 2012"—Project AB-NANOTECH, and by the University of Padova funded project: CPDA128318/12 "Study of the catalytic activity of complex graphene nanoarchitectures from ideal to real conditions". We thank CINECA for the computational support through the LISA-grant 2014: LI03p_CBC4FC.

Keywords: C–H activation · density functional calculations · organic electronics · surfaces and interfaces · Ullmann reaction

[1] J. R. Heath, *Annu. Rev. Mater. Res.* **2009**, *39*, 1 – 23.
[2] Q. Ye, C. Chi, *Chem. Mater.* **2014**, *26*, 4046 – 4056.
[3] L. Chen, Y. Hernandez, X. Feng, K. Müllen, *Angew. Chem. Int. Ed.* **2012**, *51*, 7640 – 7654; *Angew. Chem.* **2012**, *124*, 7758 – 7773.
[4] T. Weil, T. Vosch, J. Hofkens, K. Peneva, K. Müllen, *Angew. Chem. Int. Ed.* **2010**, *49*, 9068 – 9093; *Angew. Chem.* **2010**, *122*, 9252 – 9278.
[5] S. Mohnani, D. Bonifazi, *Coord. Chem. Rev.* **2010**, *254*, 2342 – 2362.
[6] K. Müllen, *ACS Nano* **2014**, *8*, 6531 – 6541.
[7] L. Bartels, *Nat. Chem.* **2010**, *2*, 87 – 95.
[8] J. V. Barth, *Annu. Rev. Phys. Chem.* **2007**, *58*, 375 – 407.
[9] A. Kühnle, *Curr. Opin. Colloid Interface Sci.* **2009**, *14*, 157 – 168.
[10] M. El Garaha, J. M. MacLeoda, F. Rosei, *Surf. Sci.* **2013**, *613*, 6 – 14.
[11] G. Franc, A. Gourdon, *Phys. Chem. Chem. Phys.* **2011**, *13*, 14283 – 14292.
[12] M. Lackinger, W. M. Heckl, *J. Phys. D* **2011**, *44*, 464011.
[13] M. Treier, C. A. Pignedoli, T. Laino, R. Rieger, K. Müllen, D. Passerone, R. Fasel, *Nat. Chem.* **2011**, *3*, 61 – 67.
[14] F. Hanke, S. Haq, R. Ravaland, M. Persson, *ACS Nano* **2011**, *5*, 9093 – 9103.
[15] S. Fischer, A. C. Papageorgiou, J. A. Lloyd, S. C. Oh, K. Diller, F. Allegretti, F. Klappenberger, A. P. Seitsonen, J. Reichert, J. V. Barth, *ACS Nano* **2014**, *8*, 207 – 215.
[16] J. Méndez, M. F. López, J. A. Martín-Gago, *Chem. Soc. Rev.* **2011**, *40*, 4578 – 4590.
[17] L. Lafferentz, V. Eberhardt, C. Dri, C. Africh, G. Comelli, F. Esch, S. Hecht, L. Grill, *Nat. Chem.* **2012**, *4*, 215 – 220.
[18] W. Wang, X. Shi, S. Wang, M. A. Van Hove, N. Lin, *J. Am. Chem. Soc.* **2011**, *133*, 13264 – 13267.
[19] R. Gutzler, H. Walch, G. Eder, S. Kloft, W. M. Hecklab, M. Lackinger, *Chem. Commun.* **2009**, 4456 – 4458.
[20] Q. Fan, C. Wang, Y. Han, J. Zhu, W. Hieringer, J. Kuttner, G. Hilt, J. M. Gottfried, *Angew. Chem. Int. Ed.* **2013**, *52*, 4668 – 4672; *Angew. Chem.* **2013**, *125*, 4766 – 4770.
[21] M. Di Giovannantonio, M. El Garah, J. Lipton-Duffin, V. Meunier, L. Cardenas, Y. F. Revurat, A. Cossaro, A. Verdini, D. F. Perepichka, F. Rosei, G. Contini, *ACS Nano* **2013**, *7*, 8190 – 8198.
[22] J. Eichhorn, D. Nieckarz, O. Ochs, D. Samanta, M. Schmittel, P. J. Szabelski, M. Lackinger, *ACS Nano* **2014**, *8*, 7880 – 7889.
[23] F. Sedona, M. Di Marino, M. Sambi, T. Carofiglio, E. Lubian, M. Casarin, E. Tondello, *ACS Nano* **2010**, *4*, 5147 – 5154.
[24] A. Basagni, L. Colazzo, F. Sedona, M. Di Marino, T. Carofiglio, E. Lubian, D. Forrer, A. Vittadini, M. Casarin, A. Verdini, A. Cossaro, L. Floreano, M. Sambi, *Chem. Eur. J.* **2014**, *20*, 14296 – 14304.
[25] Q. Fan, C. Wang, L. Liu, Y. Han, J. Zhao, J. Zhu, J. Kuttner, G. Hilt, J. M. Gottfried, *J. Phys. Chem. C* **2014**, *118*, 13018 – 13025.
[26] T. Lin, X. S. Shang, J. Adisoejoso, P. N. Liu, N. Lin, *J. Am. Chem. Soc.* **2013**, *135*, 3576 – 3582.
[27] J. Cai, P. Ruffieux, R. Jaafar, M. Bieri, T. Braun, S. Blankenburg, M. Muoth, A. P. Seitsonen, M. Saleh, X. Feng, K. Müllen, R. Fasel, *Nature* **2010**, *466*, 470 – 473.
[28] Q. Chen, A. J. McDowall, N. V. Richardson, *Langmuir* **2003**, *19*, 10164 – 10171.
[29] W. Dou, N. Li, D. Guan, F. Song, H. Huang, H. Zhang, H. Li, P. He, S. Bao, Q. Chen, W. Zhou, *J. Chem. Phys.* **2007**, *127*, 224709.
[30] W. Dou, J. Zhu, Q. Liao, H. Zhang, P. He, S. Bao, *J. Chem. Phys.* **2008**, *128*, 244706.
[31] W. Dou, J. Zhu, Q. Liao, H. Zhang, P. He, S. Bao, *J. Chem. Phys.* **2008**, *128*, 244706.■■same as ref. 30? please replace or remove and renumber■■
[32] K.-H. Chung, B.-G. Koo, H. Kim, J. K. Yoon, J.-H. Kim, Y.-K. Kwon, S.-J. Kahng, *Phys. Chem. Chem. Phys.* **2012**, *14*, 7304 – 7308.
[33] C. Baldacchini, F. Allegretti, R. Gunnella, M. G. Betti, *Surf. Sci.* **2007**, *601*, 2603 – 2606.
[34] O. McDonald, A. A. Cafolla, Z. Li, G. Hughes, *Surf. Sci.* **2006**, *600*, 1909 – 1916.
[35] R. Gutzler, L. Cardenas, J. Lipton-Duffin, M. El Garah, L. E. Dinca, C. E. Szakacs, C. Fu, M. Gallagher, M. Vondráček, M. Rybachuk, D. F. Perepichka, F. Rosei, *Nanoscale* **2014**, *6*, 2660 – 2668.
[36] J. Björk, F. Hanke, S. Stafström, *J. Am. Chem. Soc.* **2013**, *135*, 5768 – 5775.
[37] J. Bushell, A. F. Carley, M. Coughlin, P. R. Davies, D. Edwards, D. J. Morgan, M. Parsons, *J. Phys. Chem. B* **2005**, *109*, 9556 – 9566.
[38] S. U. Nanayakkara, E. C. H. Sykes, L. C. Fernández-Torres, M. M. Blake, P. S. Weiss, *Phys. Rev. Lett.* **2007**, *98*, 206108.
[39] A. Menzel, K. Swamy, R. Beer, P. Hanesch, E. Bertel, U. Birkenheuer, *Surf. Sci.* **2000**, *454*, 88 – 93.
[40] C. Y. Nakakura, E. I. Altman, *J. Vac. Sci. Technol. A* **1997**, *15*, 2359 – 2368.
[41] R. P. Vasquez, *Surf. Sci. Spectra* **1993**, *2*, 144 – 148.

[42] Y. Wang, S. Fabris, T. W. White, F. Pagliuca, P. Moras, M. Papagno, D. Topwal, P. Sheverdyaeva, C. Carbone, M. Lingenfelder, T. Classen, K. Kern, G. Costantini, *Chem. Commun.* **2012**, *48*, 534 – 536.
[43] A. Barinov, O. B. Malcioglu, S. Fabris, T. Sun, L. Gregoratti, M. Dalmiglio, M. Kiskinova, *J. Phys. Chem. C* **2009**, *113*, 9009 – 9013.
[44] T. Susi, M. Kaukonen, P. Havu, M. P. Ljungberg, P. Ayala, E. I. Kauppinen, *Beilstein J. Nanotechnol.* **2014**, *5*, 121 – 132.
[45] L. Zhang, Y. Ye, D. Cheng, H. Pan, J. Zhu, *J. Phys. Chem. C* **2013**, *117*, 9259 – 9265.
[46] A. Siokou, F. Ravani, S. Karakalos, O. Frank, M. Kalbac, C. Galiotis, *Appl. Surf. Sci.* **2011**, *257*, 9785 – 9790.
[47] Q. Sun, C. Zhang, H. Kong, Q. Tan, W. Xu, *Chem. Commun.* **2014**, *50*, 11825 – 11828.
[48] A. L. Pinardi, G. Otero-Irurueta, I. Palacio, J. I. Martinez, C. Sanchez-Sanchez, M. Tello, C. Rogero, A. Cossaro, A. Preobrajenski, B. Gomez-Lor, A. Jancarik, I. G. Stara, I. Stary, M. F. Lopez, J. Mendez, J. A. Martin-Gago, *ACS Nano* **2013**, *7*, 3676 – 3684.
[49] a) Y. Avlasevich, K. Müllen, *Chem. Commun.* **2006**, 4440 – 4442; b) A. M. Müller, Y. S. Avlasevich, W. W. Schoeller, K. Müllen, C. J. Bardeen, *J. Am. Chem. Soc.* **2007**, *129*, 14240 – 14250.
[50] I. Hamada, M. Otani, *Phys. Rev. B* **2010**, *82*, 153412.
[51] P. Giannozzi, S. Baroni, N. Bonini, M. Calandra, R. Car, C. Cavazzoni, D. Ceresoli, G. L. Chiarotti, M. Cococcioni, I. Dabo, et al., *J. Phys.: Condensed Matter* **2009**, *21*, 395502.

Received: October 26, 2014
Published online on ■■ ■■, 0000

FULL PAPER

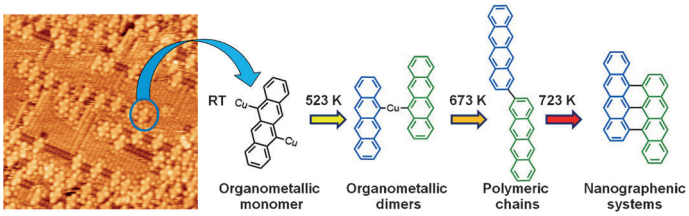

Scratching the surface: Easy control of the intermolecular coupling of 5,11-dibromotetracene on a Cu(110) surface by temperature has been achieved. Organometallic oligomers characterized by copper atoms that bridge the tetracene molecule in the 5,11 positions are formed at mild temperature (room temperature to 523 K), whereas the higher intrinsic stability of the radical sites at the 3,2 and 8,9 positions determines the formation of linear chains produced by C–C coupling between the ends of the molecules at higher temperature (see picture).

Surface Chemistry

L. Ferrighi, I. Píš, T. H. Nguyen, M. Cattelan, S. Nappini, A. Basagni, M. Parravicini, A. Papagni, F. Sedona, E. Magnano, F. Bondino, C. Di Valentin, S. Agnoli**

■■ – ■■

Control of the Intermolecular Coupling of Dibromotetracene on Cu(110) by the Sequential Activation of C–Br and C–H bonds